Tight-binding study of electron-hole pair condensation in graphene bilayers: Gate control and system-parameter dependence

D. Basu,[1] L. F. Register,[1] Dharmendar Reddy,[1] A. H. MacDonald,[2] and S. K. Banerjee[1]
[1]*Microelectronics Research Center, The University of Texas at Austin, 10100 Burnet Road, Building 160, MER 1.606B/R9900, Austin, Texas 78758-4445, USA*
[2]*Department of Physics, The University of Texas at Austin, 1 University Station C1600, Austin, Texas 78712-0264, USA*
(Received 4 May 2010; revised manuscript received 17 June 2010; published 10 August 2010)

The theoretical prediction of high-temperature electron-hole pair condensation when two graphene layers are separated by a thin dielectric film has motivated experimental work which aims to observe this condensate, and theoretical work which explores how its collective behavior could be used to design beyond-CMOS low-power electronic logic devices. Here we use a π-band tight binding model combined with Fock mean-field theory to explore the condensate properties. We study the effects of charge density, dielectric permittivity, interlayer separation, and temperature, on the formation and strength of the condensate. We model the weakening and eventual collapse of the condensate with increasing charge imbalance between layers, a mechanism which has been proposed for beyond-CMOS switching based on condensate control. Finally, we explore critical currents in the weak-coupling limit. We demonstrate that the critical current is extremely sensitive to the strength and character of interlayer tunneling processes, especially when these are weak.

DOI: 10.1103/PhysRevB.82.075409 PACS number(s): 73.21.−b, 71.35.−y, 71.10.−w, 74.25.Sv

I. INTRODUCTION

Recently it was predicted that exciton condensation could occur in a system consisting of two graphene monolayers that have equal density electron and hole carrier populations and are separated by a thin dielectric layer, and that it could survive perhaps up to and above room temperature under suitable conditions.[1,2] The resulting interlayer phase coherence due to the exciton condensate state supports many-body enhanced low-bias interlayer tunneling, as established experimentally for semiconductor bilayers at low-temperatures and in a strong magnetic field.[3,4] High-temperature condensation is favored by a synergy of favorable graphene properties:[1,2,5] the ability to use closely spaced atomically thin layers to maximize the interlayer Coulomb interaction; symmetric electron and hole band structures over the energy ranges of interest that allow accurate nesting between the electron and hole [two-dimensional (2D)] Fermi surfaces, a zero band gap which allows all of any interlayer electrostatic potential difference to be used to induce electrons and holes, and a low density of states that leads to the desired high Fermi energies at relatively low carrier densities. The possibility of room temperature condensation, the enhanced low-bias tunneling expected in the many-body ordered state, and the possible gate control thereof, has already prompted a design proposal for an extremely low-power logic device, called a bilayer pseudospin field-effect transistor (BiSFET), which could advance the international technology roadmap for semiconductors.[6,7] Although not a simple drop-in replacement for metal-oxide-semiconductor field-effect transistors (MOSFETs), SPICE-based circuit modeling[8] has demonstrated the possibility of creating a variety of logic elements with such devices with switching energies per device on the order of 0.01 aJ—i.e., 10 zepto-Joules (zJ)—discounting parasitics, if such condensates can be formed and controlled.[6,9,10] By comparison, "end of the roadmap" complementary metal-oxide-semiconductor (CMOS) is expected to have switching energies of roughly 5 aJ.[7] The qualitative advantages of this collective device concept flow from its use of gates to control collective rather than individual electron transport. The BiSFET is currently only a concept based on novel physics predicted in a novel materials system, however. If such a device and/or other devices based on such a condensate are to be realized, the conditions under which this condensate can be created and controlled must be better understood.

Here, we attempt to make progress in this direction by exploring aspects of the condensate that can be addressed under equilibrium conditions and within the mean-field Hartree-Fock approximation used in the original work, using a π-band tight binding model to extend the range of properties that can be explored. We study the sensitivity of the condensate to engineerable system parameters, exhibiting that the dielectric requirements are quite different than those of, e.g., graphene-based MOSFETs, or MOSFETs in general. We explore the effects of charge imbalance, which was proposed as a condensate control variable for the BiSFET. And we also explore the interlayer critical currents within the weak-coupling limit, demonstrating that achieving control over interlayer tunneling processes will be an important challenge in fabricating electronic devices based on bilayer graphene exciton condensates.

To the latter end, we note that when single-particle interlayer coupling is neglected entirely, the total electronic energy E_{tot} in the presence of the nearly "spontaneously formed" condensate remains independent of the global interlayer phase difference between the layers, ω. However, interlayer coherence is never truly spontaneous, but rather is influenced by other processes such as single-particle tunneling between layers, which introduces an ω dependence to E_{tot}. This feature of bilayer exciton condensate physics plays an essential role because it leads to dramatically enhanced interlayer currents up to a critical value.[11–13] When the interlayer phase stiffness is large, the critical current is given by the maximum value of the collective interlayer current,[14]

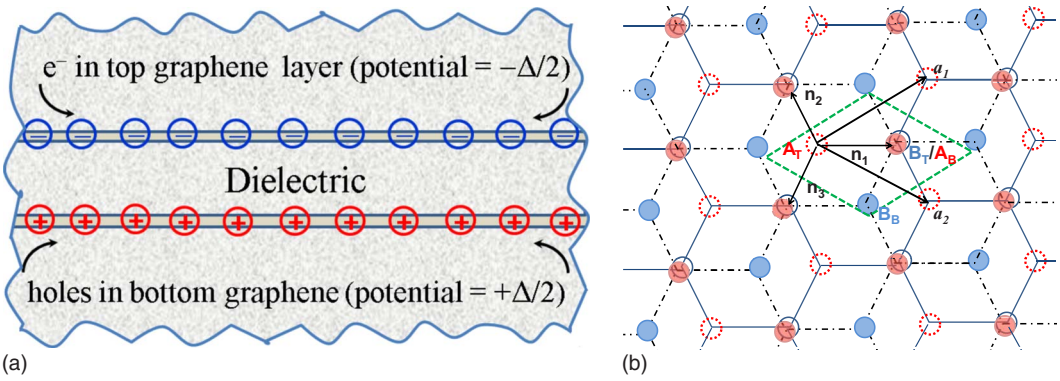

FIG. 1. (Color online) (a) Schematic of the two oppositely charged graphene monolayers, separated by a dielectric. (b) Arrangement of C atoms showing the primitive cell (green rhombus) containing four atoms—A_T (dotted circle) and B_T (blue circle) for the top layer C atoms, and A_B (red solid circle) and B_B (blue solid circle) for the bottom layer. This figure is for the Bernal stacking arrangement in which B_T lies directly above A_B. Also shown are the real space lattice vectors $\vec{a}_1$ and $\vec{a}_2$, and the vectors from A_T to the nearest neighbor B_T atoms, $\vec{n}_1$, $\vec{n}_2$, and $\vec{n}_3$.

$$I_c = (e/2\hbar)(\partial E_{\rm tot}/\partial\omega). \tag{1}$$

When the layer degree of freedom in a bilayer is viewed as a pseudospin, Eq. (1) can be viewed as a Landau-Liftshitz equation for the time-derivative of the pseudospin component which measures layer polarization. An interesting aspect of graphene bilayer condensate physics is that the collective current is sensitive to the details of the single particle interlayer coupling. We illustrate this dependence by performing explicit calculations for the weak Bernal-like and hexagonal-like bare interlayer coupling arrangements.

Our paper is organized as follows: In Sec. II, we explain the bilayer graphene tight-binding model we use within mean-field theory. In Sec. III, simulation results are presented exhibiting the detailed nature of the self-consistent exchange potentials, characterizing the dependence of the self-consistent band gap on various system parameters and on carrier imbalance such as would be achieved through gate control, and exploring the critical interlayer current within the weak coupling limit. In Sec. IV, concluding remarks are provided.

II. π-BAND COHERENT BILAYER MODEL

The bilayer graphene model system we study is shown schematically in Fig. 1(a). The arrangement of the carbon (C) atoms in the primitive cell of the two coupled graphene layers is shown in Fig. 1(b). A uniform relative dielectric constant ε_r is assumed as a first simple approximation to the net effect of interlayer and gate dielectrics and gate-induced screening. We start by neglecting the role of direct/bare single-particle hopping between layers. The only interaction between the two layers at this stage is the Coulomb attraction between electrons in one layer and holes in its neighbor. The solutions thus obtained may only be applicable in the weak direct coupling limit of course. For the purpose of definiteness, we have assumed Bernal alignment between the two layers in the relative spatial arrangement of the atoms in most cases [B sublattice atom in top layer (B_T) located above A sublattice atom in the bottom layer (A_B)]. However, our results do not change significantly—quantitatively or qualitatively—if the two layers are aligned hexagonally (A_T above A_B, and B_T on top of B_B).

Within Hartree-Fock (HF) theory many-body interactions are approximated by a non-local mean field potential $V_{\rm HF}(\mathbf{R_1},\mathbf{R_2})$ for the electrons. Note that all of our explicit calculations are performed in terms of the electrons in both layers, rather than considering holes in the p-type layer. This potential can be written as the sum of three distinct potentials[15] which are

$$V_{\rm HF}(\mathbf{R}_1,\mathbf{R}_2) = \delta(\mathbf{R}_1,\mathbf{R}_2)V_{ext}(\mathbf{R}_1) + \delta(\mathbf{R}_1,\mathbf{R}_2)\sum_{\mathbf{R}_3}\frac{e^2}{4\pi\varepsilon_0\varepsilon_r|\mathbf{R}_1-\mathbf{R}_3|}\sum_\beta n_\beta|\varphi_\beta(\mathbf{R}_3)|^2 - \frac{e^2}{4\pi\varepsilon_0\varepsilon_r|\mathbf{R}_1-\mathbf{R}_2|}\sum_\beta n_\beta\varphi_\beta(\mathbf{R}_1)\varphi^*_\beta(\mathbf{R}_2), \tag{2}$$

on our tight binding lattice, where $\mathbf{R}$ are the positions of the atoms, φ_β are the tight-binding electron energy eigenfunctions, and n_β are the occupancy factors, and the $\delta(\mathbf{R}_1,\mathbf{R}_2)$ are Kronecker delta functions in the discrete coordinates $\mathbf{R}$. The first two terms are local, arising from the external field and the local charge density (Hartree potential) respectively, and the last term is the nonlocal Coulomb-mediated exchange potential (Fock potential).

For this study of excitonic condensation in graphene bilayers, we are primarily interested in the interlayer exchange interaction,

$$V_{\rm HF}(\mathbf{R}_T,\mathbf{R}_B) = \frac{-e^2}{4\pi\varepsilon_0\varepsilon_r\sqrt{(\Delta R)^2+d^2}}\sum_{\alpha,\mathbf{k},s} n_{\alpha,\mathbf{k},s}\varphi_{\alpha,\mathbf{k},s}(\mathbf{R}_T) \times\varphi^*_{\alpha,\mathbf{k},s}(\mathbf{R}_B). \tag{3}$$

Here $\mathbf{R}_T$ and $\mathbf{R}_B$ are the 2D in-plane vectors for the atoms in the top and bottom graphene layers, respectively. $\Delta R=|\mathbf{R}_T-\mathbf{R}_B|$ is the magnitude of the in-plane component of the separation between the atoms, and d is the separation between the two layers. And the eigenstates label β has been expanded in terms of the band index α, wave vector $\mathbf{k}$, and

spin state s. The remaining potential, the Hartree terms and the intralayer Fock terms serve to self-consistently determine the gate potentials which would be required to introduce a specific potential difference between the top and bottom layers. In this work, we represent these latter contributions simply by assuming a potential difference Δ, such that a $\mp\Delta/2$ potential is added to the top (electron) and bottom (hole) layers, respectively.

A self-consistent solution for $V_{\mathrm{HF}}(\mathbf{R}_T,\mathbf{R}_B)$ within an effective single-particle tight-binding Schrodinger equation is sought to approximate the true many-body ground state. For each value of α, $\mathbf{k}$, s, this Schrodinger equation can be written as:

$$H_{TB}\varphi_{\alpha,\mathbf{k},s}(\mathbf{R}_T) - (\Delta/2)\varphi_{\alpha,\mathbf{k},s}(\mathbf{R}_T) + \sum_{\mathbf{R}_B} V_{\mathrm{HF}}(\mathbf{R}_T,\mathbf{R}_B)\varphi_{\alpha,\mathbf{k},s}(\mathbf{R}_B) = \varepsilon_{\alpha,\mathbf{k},s}\varphi_{\alpha,\mathbf{k},s}(\mathbf{R}_T) \tag{4a}$$

and

$$H_{TB}\varphi_{\alpha,\mathbf{k},s}(\mathbf{R}_B) + (\Delta/2)\varphi_{\alpha,\mathbf{k},s}(\mathbf{R}_B) + \sum_{\mathbf{R}_T} V_{\mathrm{HF}}(\mathbf{R}_B,\mathbf{R}_T)\varphi_{\alpha,\mathbf{k},s}(\mathbf{R}_T) = \varepsilon_{\alpha,\mathbf{k},s}\varphi_{\alpha,\mathbf{k},s}(\mathbf{R}_B) \tag{4b}$$

for the top and bottom layers, respectively. Here, ε are the eigenenergies and H_{TB} is the nearest neighbor π-orbital (p_z-orbital for the assumed x-y oriented graphene planes) tight-binding Hamiltonian from which the single particle band structure is obtained using

$$H_{TB}\varphi_{\alpha,\mathbf{k},s}(\mathbf{R}) = t\sum_j \varphi_{\alpha,\mathbf{k},s}(\mathbf{R}_j), \tag{5}$$

where $t=-2.7$ eV.[16] Note that $\varphi_{\alpha,\mathbf{k},s}(\mathbf{R})$ for any atom located at $\mathbf{R}''$ outside the four-atom primitive unit cell of the bilayer graphene system can be obtained from the value for the corresponding atom with the primitive unit cell $\mathbf{R}'$ by using the Bloch condition $\varphi_{\alpha,\mathbf{k},s}(\mathbf{R}'')=e^{i\mathbf{k}\cdot(\mathbf{R}''-\mathbf{R}')}\varphi_{\alpha,\mathbf{k},s}(\mathbf{R}')$.

Self-consistent solutions to Eqs. (3), (4a), (4b), and (5) can be obtained simply by setting the Coulomb-mediated interlayer exchange interaction of Eq. (3) to zero. This solution corresponds to an uncorrelated state with electrons isolated in one layer or the other, and bands in the two layers simply shifted by $\mp\Delta/2$. A self-consistent solution of Eqs. (3), (4a), (4b), and (5) that yields a nonzero value of the interlayer exchange potential and eigenfunctions that are coherent sums of orbital amplitudes on both layers captures the condensate state.[13] As usual these solutions of the Hartree-Fock equations minimize the total energy subject to the Slater determinant wave-function approximation. When bare interlayer tunneling terms are absent in the Hamiltonian, the state with interlayer coherence, and therefore interaction terms in the mean-field Hamiltonian that act like interlayer hopping/tunneling potentials for the Hartree-Fock quasiparticle, break the Hamiltonian symmetry which conserves particle number separately in each layer. The broken symmetry state has lower interlayer Coulomb interaction energy because the anti-symmetry of the many-electron wave-function reduces the spatial overlap probability between electrons in different layers only when coherence is present. In terms of the quasi-particle energy spectrum, a gap is formed in the band structure of the two-layer system about the points at which the conduction band of the top layer and the valence band of the bottom layer would otherwise cross. With the Fermi level in the vicinity of this anticrossing, the energy reduction for the condensed state can be seen in the reduction of the energies of the occupied Hartree-Fock quasiparticle states in the vicinity of the anti-crossing.

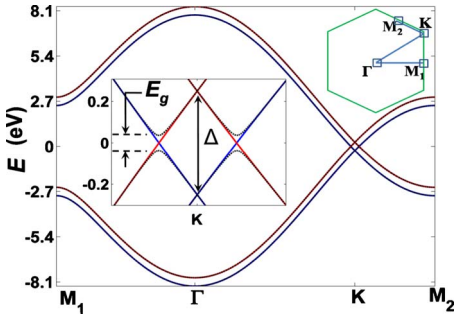

FIG. 2. (Color online) Energy bands of two graphene layers separated by 1.0 nm of SiO_2 (ε_r=3.9), having layer potentials of $-\Delta/2$ (top layer—blue) and $+\Delta/2$ (bottom layer—red) in the uncoupled state (solid lines) along the high symmetry directions in the Brillouin zone (shown above). Δ=0.5 eV. Phase coherence between layers creates a correlated, lower energy state (black dash-dotted lines). The inset magnifies the low energy spectrum, revealing a band gap E_g of 74 meV at 0 K for balanced top and bottom layer charge distributions, i.e., E_F is located within the band gap in this case.

For illustration, this gap formation for the correlated state at 0 K temperature with balanced charge distributions of 6×10^{12} cm^{-2} corresponding to an interlayer potential splitting Δ of 0.5 eV, with an interlayer spacing of 1 nm, and with a dielectric permittivity ε_r=3.9 of SiO_2 is shown in Fig. 2 where the quasi-particle energy bands are plotted along the high-symmetry directions. The size of the gap in this case is ~30% of the isolated layer Fermi energies relative to their respective Dirac points.

To obtain this and subsequent correlated state solutions numerically, we used an iterative procedure and "seeded" the calculations for the first iteration only either by re-

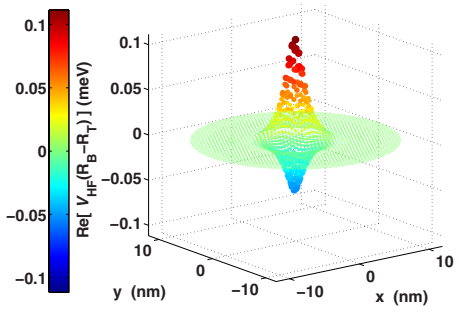

FIG. 3. (Color online) The real-space variation of the exchange potential $V_{\mathrm{HF}}(\mathbf{R}_T,\mathbf{R}_B)$ for coupling between atoms of the A sublattices of top and bottom layers, as a function of $\mathbf{R}_B-\mathbf{R}_T$. Δ=0.5 eV, d=1 nm, ε_r=3.9, and balanced charge distributions at 0 K are assumed. Here and in Figs. 4–6 below, the color of the marker spheres indicate the value of the interaction, and the sizes of the spheres indicate the magnitude of this value.

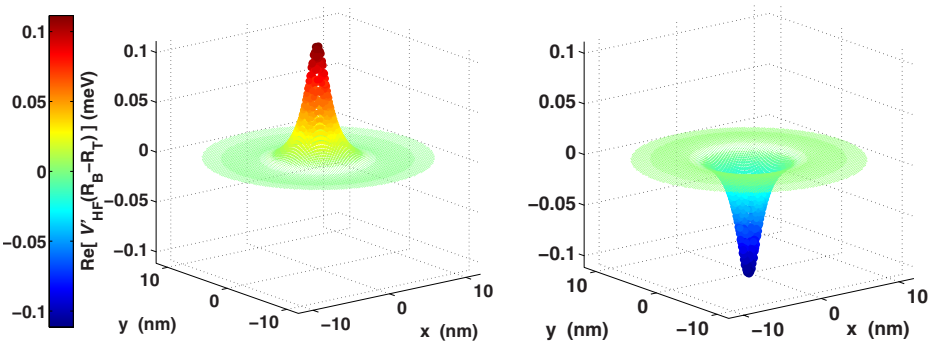

FIG. 4. (Color online) $V'_{\mathrm{HF}}(\mathbf{R}_T,\mathbf{R}_B)$ for (left) A_T-A_B coupling and (right) B_T-B_B coupling, obtained by dividing $V_{\mathrm{HF}}(\mathbf{R}_T,\mathbf{R}_B)$ by $\exp[i\mathbf{k}_D(\mathbf{R}_B-\mathbf{R}_T)]$, as a function of $\mathbf{R}_B-\mathbf{R}_T$. The imaginary components vanish. $\Delta=0.5$ eV, $d=1$ nm, $\varepsilon_r=3.9$, and balanced charge distributions at 0 K are assumed.

placing the tight-binding wave-function correlation product $\phi_{\alpha,\mathbf{k},s}(\mathbf{R}_T)\phi^*_{\alpha,\mathbf{k},s}(\mathbf{R}_B)$ in Eq. (3) by $c\exp[i\mathbf{k}(\mathbf{R}_T-\mathbf{R}_B)$ where c is a small dimensionless constant; by replacing the exchange interaction of Eq. (3) with a Bernal-like or hexagonal-like but weaker bare interlayer coupling; or by starting from a self-consistent condensate state obtained previously under different conditions. In any case, for subsequent iterations the seed was removed and the Fock potential of Eq. (3) was obtained from the wave-functions of the previous iteration, and the calculation was iterated until convergence was achieved. We emphasize that we have confirmed through multiple tests that the final self-consistent solutions are not dependent on this initial seeding method or value.

III. RESULTS AND DISCUSSION

A. Real-space characteristics of the nonlocal exchange potential

The non-local mean-field exchange interaction appears as an effective interlayer hopping term in the tight-binding Hamiltonian. For conceptual understanding, it is convenient to subdivide interlayer exchange into four contributions distinguished by sublattice indices for both top and bottom layers. Coupling between an A sublattice atom in the top layer and an A sublattice atom in the bottom layer can be identified as an A_T-A_B interaction. Similarly A_T-B_B, B_T-A_B, and B_T-B_B interactions can be identified.

The non-local nature of the exchange interaction is evident from the self-consistently calculated A_T-A_B exchange potential shown in Fig. 3, obtained under the same conditions as given above for Fig. 2. The rapidly oscillating dependence of this nonlocal potential on $\mathbf{R}_B-\mathbf{R}_T$ is apparent from the positive and negative excursions of the potential in Fig. 3. The picture becomes simpler if the contributions to $V_{\mathrm{HF}}(\mathbf{R}_T,\mathbf{R}_B)$ from states near the two Dirac points $\mathbf{k}_D$ are considered separately. (We have confirmed that the exchange potential contribution from near one Dirac point has little effect on quasiparticles near the other Dirac point, as assumed from the beginning in continuum model theories.) When we divide out the phase factor $\exp[i\mathbf{k}_D(\mathbf{R}_B-\mathbf{R}_T)]$ from the $V_{\mathrm{HF}}(\mathbf{R}_T,\mathbf{R}_B)$ contribution from near one or the other Dirac point $\mathbf{k}_D$, we obtain the potential $V'_{\mathrm{HF}}(\mathbf{R}_T,\mathbf{R}_B)$, illustrated in Fig. 4 for A_T-A_B and B_T-B_B interactions. To within the arbitrary constant phase factor for $V'_{\mathrm{HF}}(\mathbf{R}_T,\mathbf{R}_B)$ as a whole discussed above, the resulting functions A_T-A_B and B_T-B_B can be taken as purely real. Furthermore, the eigenstates of the coupled system $\varphi_{\alpha,\mathbf{k},s}$ that contribute most to the exchange interaction are necessarily those that significantly overlap both layers, those near the band anticrossing centered about the nominal Fermi surface $k_F=|\mathbf{k}_F-\mathbf{k}_D|$ location for the uncoupled system for these balanced charge distributions. The calculated exchange interaction decays not only with the large characteristic Coulomb decay of $(\Delta R^2+d^2)^{-1/2}$, but also with spatial correlation of the condensate which, for typical gaps in these calculations for coupled graphene layers, has a characteristic scale of $\Delta R\sim k_F^{-1}$.

The functions $V'_{\mathrm{HF}}(\mathbf{R}_T,\mathbf{R}_B)$ for A_T-A_B and B_T-B_B, while of identical magnitude, are of opposite sign. This result is expected because conduction and valence band (pseudo-) spinors at a given wave vector differ only by the relative sign of their projections onto individual sublattices. This self-consistent coupling we obtain is of the form required to maximize the interaction between conduction band states in one layer and valence band states in the other layer. However, as evident from Figs. 5 and 6, $V'_{\mathrm{HF}}(\mathbf{R}_T,\mathbf{R}_B)$ for A_T-B_B and B_T-A_B coupling are complex functions of $\mathbf{R}_B-\mathbf{R}_T$ and have peak values that are quite a bit smaller than the A_T-A_B and B_T-B_B couplings, having only about one-fifth of the peak magnitude. Due to the chiral nature of graphene, the relative

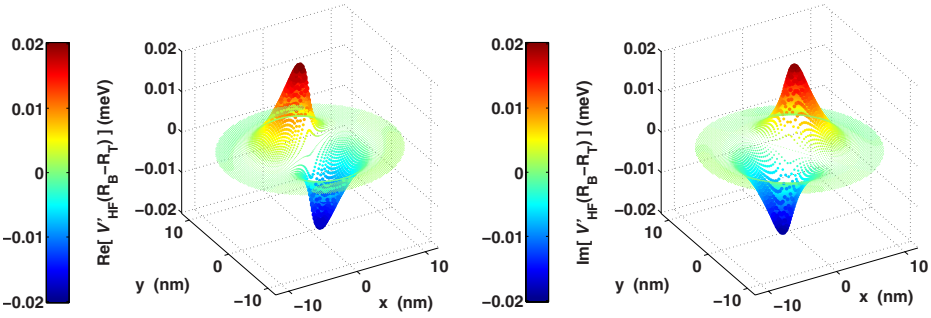

FIG. 5. (Color online) (Left) Real and (right) imaginary parts of $V'_{\mathrm{HF}}(\mathbf{R}_T,\mathbf{R}_B)$ for A_T-B_B coupling as a function of $\mathbf{R}_B-\mathbf{R}_T$. $\Delta=0.5$ eV, $d=1$ nm, $\varepsilon_r=3.9$, and balanced charge distributions at 0 K are assumed.

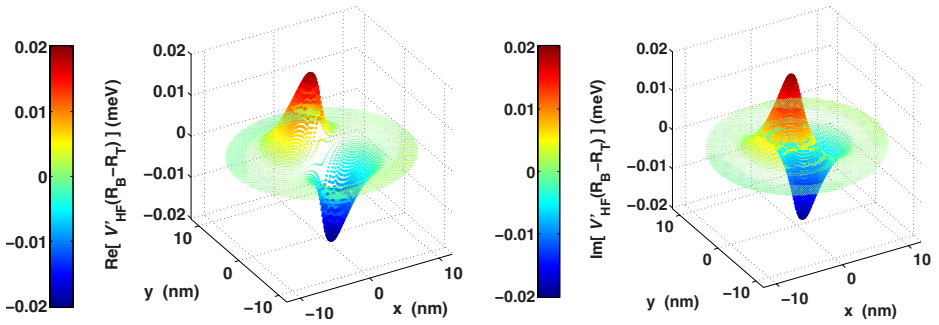

FIG. 6. (Color online) (Left) Real and (right) imaginary parts of $V'_{\mathrm{HF}}(\mathbf{R}_T,\mathbf{R}_B)$ for B_T-A_B coupling as a function of $\mathbf{R}_B-\mathbf{R}_T$. $\Delta=0.5$ eV, $d=1$ nm, $\varepsilon_r=3.9$, and balanced charge distributions at 0 K are assumed.

phases of the wave functions on the A and B sublattices of each layer also vary rapidly with $\mathbf{k}$ around the Fermi surface. As a result, even for small ΔR, the mostly constructive phase interference among contributions of individual states $\varphi_{\alpha,\mathbf{k},s}$ to $V'_{\mathrm{HF}}(\mathbf{R}_T,\mathbf{R}_B)$ between A sublattice sites and between B sublattice sites, implies substantial destructive interference between the contributions to both A_T-B_B and B_T-A_B exchange potentials. We note that the mean-field interlayer coupling $V'_{\mathrm{HF}}(\mathbf{R}_T,\mathbf{R}_B)$ is quite distinct in character from any familiar single-particle interlayer coupling, whether Bernal-like or hexagonal-like. This observation will play a key role in the consideration of critical currents later.

There are also separate solutions of the mean-field equations with mostly constructive interference among the contributions for either A_T-B_B or B_T-A_B exchange potentials, but at a cost of substantial destructive interference for all three other combinations, and a corresponding weaker total coupling that is less energetically favorable, at least in the absence of bare coupling. As a result, in our self-consistent calculations of the spontaneous condensate, these solutions are unstable, as also to be expected physically.

Finally we note that shifting the bottom layer lattice slightly in real space to obtain a hexagonal spatial overlap (A_T above A_B, B_T above B_B) has essentially no effect on the exchange potentials and band structure. The spatial structure of the interlayer hopping mean field is determined almost exclusively by the sublattice structures of the wave functions at the Fermi level in the separate layers, and hardly at all by the influence of relative atomic positions on interlayer Coulomb interactions because of the large interlayer separations d as compared to interatomic distances within the layers. Even in a strongly coupled bilayer (low temperature T, low ε_r, small d) the band gaps for real-space hexagonal and Bernal atomic arrangements are equal to within fractions of meVs of one another.

B. System parameter dependence

In bilayer systems an electric potential difference between layers is necessary to induce carriers and open up the opportunity for condensation. The dependence of the coherence-induced band gap, a measure of the condensate strength, on the electric potential difference Δ is shown in Fig. 7 for three different dielectric constants and a fixed interlayer spacing d of 1 nm. Note that there is continuous strengthening of the condensate with increasing Δ. However the rate of increase is smaller at large values of Δ. This diminishing rate of return is even more pronounced when viewed as a function of electron and hole densities, which scale as Δ^2 because of the linear band structure in contrast to the Fermi energy which is equal to $\Delta/2$. On the other hand, $\Delta/2=E_F$ should remain above roughly $8k_BT$ where k_B is Boltzmann's constant, which is approximately 200 meV at room temperature.

The low-energy quasiparticle band dispersion of the two-layer graphene system is plotted in Fig. 8(a) as a function of interlayer separation d, for effective dielectric constant $\varepsilon_r=2.2$ and $\Delta=0.5$ eV. As d increases, the exchange interaction becomes weak and the band-structure approaches that of the uncoupled system. The nearly exponential dependence of the band gap on layer separation is evident from the semilog plot in Fig. 8(b), where we plot the band gap at $T=0$ K and $\Delta=0.5$ eV for two additional dielectric constant values. This strong dependence on the interaction strength, controlled by d, has the same origin as the familiar strong dependence on weak interactions in the qualitative McMillan formula for the critical temperatures of superconductors.

In Figs. 7, 8(b), and 9, we plot the condensate band gap as a function of ε_r for graphene layers separated by 1 nm, at $\Delta=0.5$ eV and $T=0$ K and $T=300$ K. These figures exhibit the weakening of the condensate with increasing ε_r and the corresponding decrease in the Coulomb interaction between the two layers. Here we note that ε_r of 2.2 is essentially that used in original work of Ref. 1 and is close to that speculated for graphene on SiO_2 in air,[17] or it can be thought of as that of a low-κ material such as BN.[18] $\varepsilon_r=3.0$ corresponds to a low-κ dielectric like C-doped SiO_2,[19] $\varepsilon_r=3.9$ corresponds to SiO_2. And $\varepsilon_r=9.1$ corresponds to a high-κ dielectric like Al_2O_3.

We note that overall the strength of the condensate is more sensitive to changes in ε_r than d, as further exhibited in

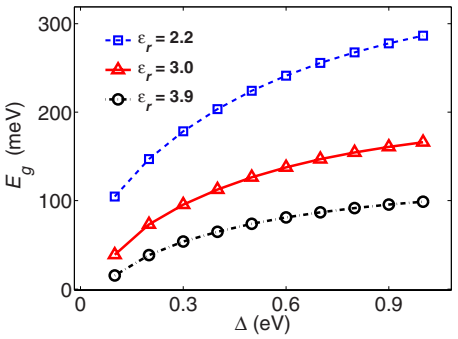

FIG. 7. (Color online) Band gap as a function of potential difference Δ for three different dielectrics, with $d=1$ nm and balanced charge distributions at 0 K.

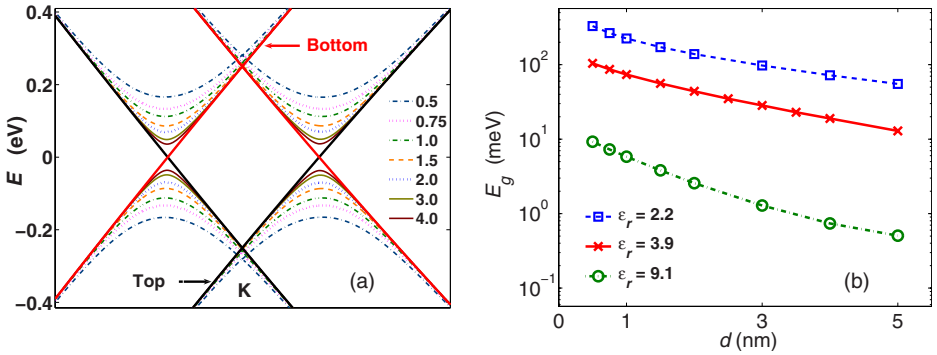

FIG. 8. (Color online) (a) Low-energy dispersion of the graphene bilayer system with $\Delta=0.5$ eV and $\varepsilon_r=2.2$ at 0 K, and balanced charge distributions, as a function of layer separation d (legend entries are in nm). The labeled solid lines (black and red online, respectively) are the band structures of the top and bottom graphene layers in absence of an exchange coupling between the layers. (b) Band gap E_g in the correlated condensate state for three different dielectrics, showing exponential scaling of the band gap with layer separation, at 0 K with $\Delta=0.5$ eV and balanced charge distributions.

Fig. 10 where the band gap is plotted as a function of both ε_r and d. For example, the gap widens by a factor of about 3.9 when ε_r decreases from 4 to 2, but only by a factor of about 1.6 when d decreases from 2 nm to 1 nm. For the nonlocal exchange potential $V_{\mathrm{HF}}(\mathbf{R}_T,\mathbf{R}_B)$ defined in Eq. (2), the underlying Coulomb interaction varies with ε_r^{-1} for all values of ΔR, but as d^{-1} only for $\Delta R=0$.

As in the theory of superconductivity, the mean-field theory condensate is destroyed by thermal energies k_BT on the order of the 0 K energy gap, E_{g0}. Specifically, for these otherwise decoupled graphene bilayers, the occupation probabilities $n_{\alpha,\mathbf{k},s}$ of the electronic states $\varphi_{\alpha,\mathbf{k},s}$ below the band gap that contribute most to $V_{\mathrm{HF}}(\mathbf{R}_T,\mathbf{R}_B)$ decrease with increasing temperature. In addition, the occupation of the states above the band gap increase in the same way, but the contributions to $V_{\mathrm{HF}}(\mathbf{R}_T,\mathbf{R}_B)$ for any occupied states $\varphi_{\alpha,\mathbf{k},s}$ above the band gap are precisely opposite to that for the corresponding state $\varphi_{\alpha,\mathbf{k},s}$ below the band gap. Both contributions, thus, weaken $V_{\mathrm{HF}}(\mathbf{R}_T,\mathbf{R}_B)$ with increasing temperature. Furthermore, as the condensate weakens, the band gap shrinks producing a positive feedback and a rapid collapse in the self-consistently calculated condensate with increasing temperature. Figure 11 shows the temperature dependence of the band gap for three different effective dielectric constants. The layer separation $d=1$ nm and the potential difference $\Delta=0.5$ eV in all cases. As expected, the lower the permittivity, the stronger the 0 K condensate, and the higher the temperature that can be tolerated. The insert in Fig. 11, where the data is scaled by E_{g0}, illustrates that the condensate decay is close to a universal function of k_BT/E_{g0} as expected for these balanced charge distributions, with collapse with temperature by $k_BT/E_{g0}\approx 0.25$, or $E_{g0}\approx 4k_BT$. Any parameter change that alters the E_{g0}/k_BT ratio is expected to produce a similar effect, as per the collapse of the condensate shown in Fig. 9 at a fixed temperature of 300 K as a function of dielectric permittivity when E_{g0} approaches 100 meV ($k_B\cdot 300$ K=25.9 meV).

Mean-field theory accounts for condensate suppression due to fermionic entropy at finite temperatures, but does not account for thermal fluctuations of the condensate spatial distribution. The latter effect dominates at very large values of E_{g0}, as explained in Ref. 1, but because of the condensate's substantial phase stiffness,[1] is expected to produce relatively small changes in critical temperature T_c at the coupling strengths that can be reached experimentally.

C. Gate control

Understanding the sensitivity of the condensate to charge imbalance may be critical to designing and interpreting ex-

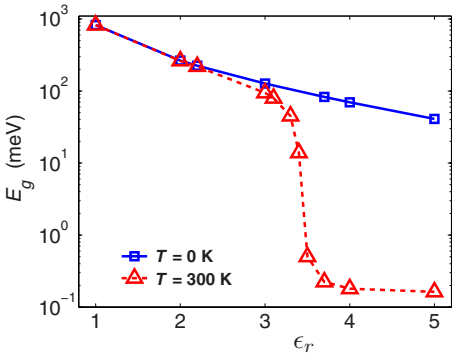

FIG. 9. (Color online) Band gap for two graphene layers with $\Delta=0.5$ eV, $d=1$ nm, and balanced charged distributions at 0 and 300 K, as a function of the dielectric constant. The minimum values are limited by the accuracy of the calculation.

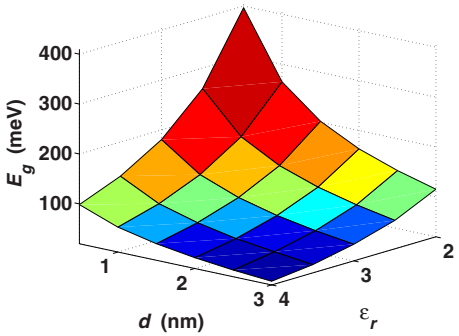

FIG. 10. (Color online) Band gap E_g for the bilayer condensate with $\Delta=0.5$ eV and balanced charged distributions at 0 K, as a function of the interlayer dielectric constant ε_r and layer separation d.

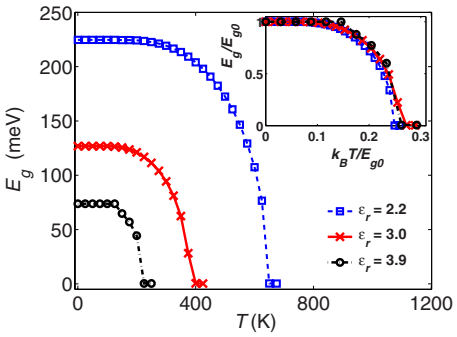

FIG. 11. (Color online) Temperature dependence of the band gap for three different dielectric constants with $\Delta=0.5$ eV, $d=1$ nm and balanced charge distributions. Lower ε_r results in larger coupling strength and therefore larger 0 K band gaps that are, therefore, also more robust at higher temperatures. The top right insert shows the same data scaled by 0 K band gap (E_{g0}), to illustrate the similarity of the T dependence of band gap for different ε_r.

periments to observe the condensate. And gate control of the condensate through its dependence on electron-hole charge imbalance provides the switching mechanism imagined in the proposed BiSFET device. Under equilibrium conditions, a charge imbalance corresponds to a shift in the Fermi energy either up or down away from the middle of the condensate's band gap. In particular, lowering the Fermi level corresponds to decreasing the electron concentration in the upper graphene layer and increasing the hole concentration in the lower layer in these simulations. The associated reduction in occupation probabilities $n_{\alpha,\mathbf{k},s}$ of the states $\varphi_{\alpha,\mathbf{k},s}$ is most pronounced for those states of the correlated system nearest to the band edge, which again are those which contribute most strongly to $V_{\mathrm{HF}}(\mathbf{R}_T,\mathbf{R}_B)$. Thus, the condensate is weakened and the band gap shrinks. For these unbalanced cases, the location of the Fermi level must be self-consistently calculated, along with changes in $V_{\mathrm{HF}}(\mathbf{R}_T,\mathbf{R}_B)$, to maintain a fixed degree of charge imbalance as would be imposed by external gating. We note that shifting the Fermi level up, corresponding to increasing the electron concentration and reducing the hole concentration, has an identical effect since the contributions of occupied states $\varphi_{\alpha,\mathbf{k},s}$ above the band gap to $V_{\mathrm{HF}}(\mathbf{R}_T,\mathbf{R}_B)$ precisely cancel out the contributions of those of their counterparts $\varphi_{\alpha,\mathbf{k},s}$ below the band gap, as previously noted.

Self-consistently calculated band edges and relative E_F positions as a function of the charge imbalance between the top electron (n) layer and bottom hole (p) layer, here defined as $(n-p)/(n+p)$, for the graphene bilayers separated by 1 nm of $\varepsilon_r=3$ low-κ material at 25 and 300 K are shown in Fig. 12. The same is shown for bilayers separated by 1.3 nm under otherwise identical conditions in Fig. 13. (We use 25 K here because, with the Fermi level now varying self-consistently with the band gap, the solutions become increasingly difficult to converge with decreasing temperatures.) We find that the condensate can be eliminated by charge balances of 25% or less in these simulations. And it can be substantially weakened at 300 K with charge variations of around 10%, which is all that would be required for the proposed BiSFET. Furthermore, though we have considered only a small region of the design space here, it appears that the weaker the initial condensate, the more sensitive it is to charge imbalance. Thus, from an applications point of view, the strongest condensate is not necessarily the best condensate.

D. Critical current

The critical current that the condensate can support is expected to depend on the bare single particle (no condensate) interlayer coupling V_{bare} as discussed in the introduction. To estimate the critical current here, we treat the bare interlayer coupling as a weak perturbation. The principal contribution to the total electronic energy E_{tot} is that due to the interlayer mean-field exchange interaction. However, this exchange interaction does not actually establish a preferred value for the phase difference ω between the layers, as previously noted. That is, the condensate properties of the otherwise uncoupled layers remain the same if the phases of the self-consistent wave-functions are uniformly modified by a phase factor $e^{i\omega}$ in one layer. Therefore, the global interlayer phase (ω) dependence of the total electronic energy E_{tot} of Eq. (1) reduces to the ω dependence of the expectation value of the corresponding single-particle coupling Hamiltonian contribution, V_{bare}, here calculated to first order in terms of the wave-functions of the unperturbed condensate state. This expectation value is,

$$\langle V_{\mathrm{bare}}\rangle = \sum_{\alpha,\mathbf{k},s} (\Delta_{\mathbf{k}}/A_{BZ}) n_{\alpha,\mathbf{k},s} \langle \phi_{a,\mathbf{k},s}|V_{\mathrm{bare}}|\phi_{a,\mathbf{k},s}\rangle, \qquad (6)$$

where $\Delta_{\mathbf{k}}$ is the k-space area associated with each $\mathbf{k}$ point, and A_{BZ} is the Brillouin zone (BZ) area. The wave functions have been normalized so that $\Sigma_{\alpha,\mathbf{k},s}(\Delta_{\mathbf{k}}/A_{BZ}) n_{\alpha,\mathbf{k},s}\langle \phi_{a,\mathbf{k},s}|\phi_{a,\mathbf{k},s}\rangle = 4$ per primitive unit cell, consistent with filling the band structure up to the Dirac

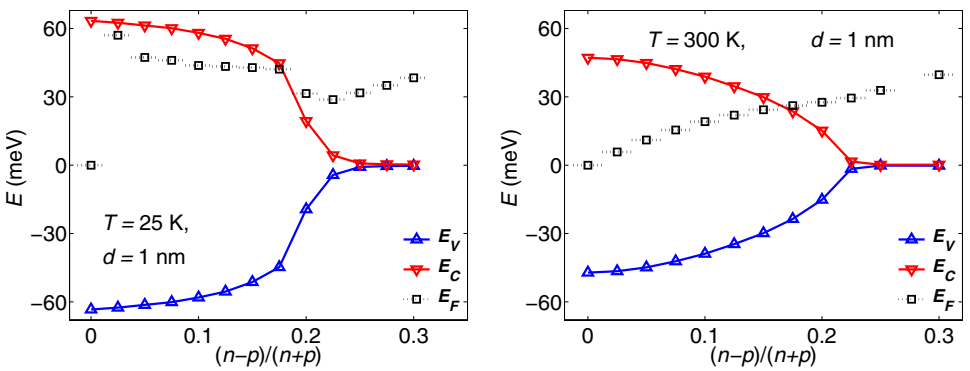

FIG. 12. (Color online) Energy band edges and Fermi level as a function of carrier imbalance between top layer electron density and bottom layer hole density for graphene bilayers at 25 and 300 K separated by 1 nm dielectric with $\varepsilon_r=3$ and $\Delta=0.5$ eV.

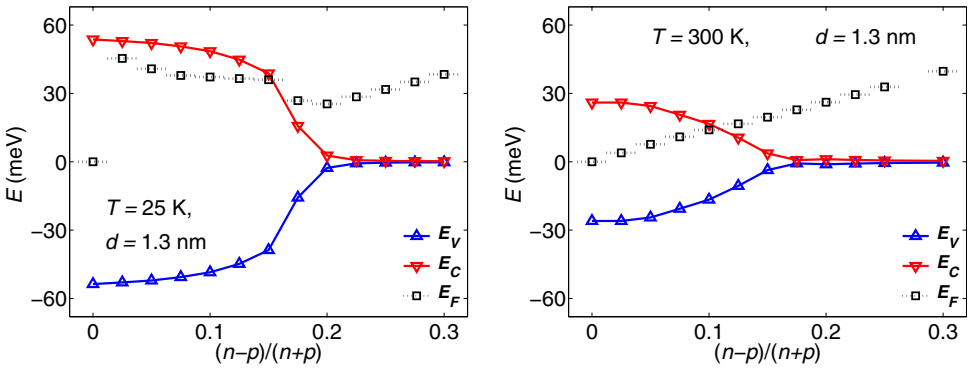

FIG. 13. (Color online) Energy band edges and Fermi level as a function of carrier imbalance between top layer electron density and bottom layer hole density for graphene bilayers at 25 and 300 K separated by 1.3 nm dielectric with $\varepsilon_r=3$ and $\Delta=0.5$ eV.

point on average. The critical current, I_c, the maximum steady-state current that can flow between the two condensates, can then be estimated from the maximum value of Eq. (1), which now takes the form $I_c=(e/2\hbar)(\partial E_{\rm tot}/\partial\omega)=(e/2\hbar)(\partial\langle V_{\rm bare}\rangle/\partial\omega)$ here (where both spin and valley degeneracy have already been accounted for in the summations above).

In the geometry that is most commonly considered, the interlayer hopping would occur across a possibly amorphous dielectric. Epitaxial tunnel barriers, such as BN for example, could offer important advantages if the relative orientations of the graphene and BN layers could be controlled[20] as will become clear from the following discussion. Both the typical size of tunneling matrix elements and the degree to which they satisfy momentum conservation could vary widely. Here, for the purpose of illustration, we treat the bare tunneling as simply a parameter. Consider first bare interlayer coupling to be $V_{\rm bare}=t_\perp$ for A_T and A_B atoms within the same bilayer primitive unit cell, and to be zero otherwise. For the condensate corresponding to 1 nm layer separation, a low-κ dielectric of $\varepsilon_r=3.0$ and an interlayer potential of $\Delta=0.5$ eV at 0 K, which produced a 127 meV band gap, we find (see Fig. 14) that the critical current is approximately $(t_\perp/\text{eV})\times(1.8\times10^{-3})\times(e/\hbar)$ per primitive cell, or $t_\perp\times8.4$ nA nm^{-2} meV^{-1}. (Expressed per nominal charge carrier per layer, electron or hole, the critical current is $(t_\perp/\text{meV})\times0.58\times(e/\hbar)$.) For a $t_\perp$ of approximately 1.2 meV this result is essentially that employed for modeling purposes for the BiSFET,[5] although even 1.2 meV is beyond the perturbative limit for these calculations. However if under the same conditions otherwise, we take $V_{\rm bare}=t_\perp$ for a B_T-A_B Bernal-like coupling within the same primitive unit cell, the critical current essentially vanishes (drops by roughly two orders of magnitude or more depending on precise details of the layer alignments). The reason for this stark difference becomes clear upon noting that the values of Fock potentials $V'_{\rm HF}(\mathbf{R}_T,\mathbf{R}_B)$ of Eq. (3)—as illustrated by Figs. 4–6—at (or at least very close to) the origin, $\mathbf{R}_B-\mathbf{R}_T=0$ are the values of the corresponding expectation values of $V_{\rm bare}$ of Eq. (6) to within a factor of $-t_\perp 4\pi\varepsilon_0\varepsilon_r d/e^2$ and the phase factor ω. As can be seen from these figures, in this way, bare A_T-A_B coupling or bare B_T-B_B will couple strongly to the condensate. In contrast bare B_T-A_B or bare A_T-B_B coupling to the condensate essentially vanishes. And the hexagonal-like in-phase sum of equal A_T-A_B and B_T-B_B coupling, which is essentially orthogonal to the condensate that is self-optimized in an "antihexagonal" manner to maximize the exchange coupling between the conduction band of one layer and the valence band of the other, as discussed previously, suffers the same fate. These stark differences demonstrate that, in this perturbative limit at least, critical currents will be sensitive not only to the thickness of the tunnel barrier but also to its detailed atomic structure and coupling to the graphene.

We emphasize that the above results were obtained in the perturbative limit when the bare coupling is quite weak and has little or no effect on the condensate itself, such as might occur in initial efforts to experimentally observe such a condensate. However, in the presence of more significant if still moderate bare A_T-A_B or B_T-A_B coupling for example, the energetically favorable solutions for the combined Hamiltonian could take on this latter character, which would have a profound effect on the corresponding critical currents.

IV. CONCLUSION

Recently it was predicted that exciton condensation could occur in a system consisting of two graphene monolayers

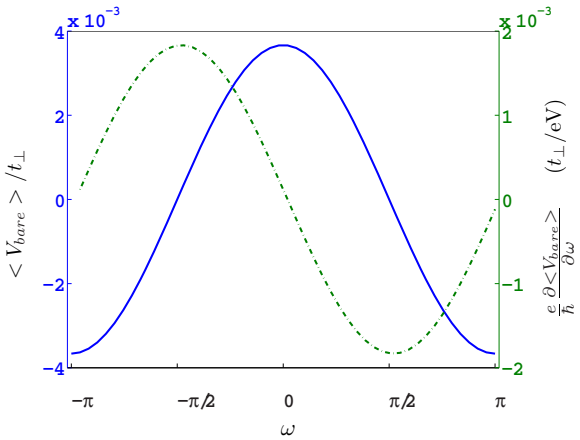

FIG. 14. (Color online) Expectation value of the interlayer tunneling $\langle V_{\rm bare}\rangle$ expressed in terms of the assumed bare interlayer tunneling $t_\perp$, as a function of the interlayer phase difference ω (left axis, blue solid curve). Right axis (green dotted curve) shows the critical current. Both results are for interlayer bare tunneling between only A_T and A_B carbon atoms. $\langle V_{\rm bare}\rangle$ as well as the critical current approaches zero for Bernal-like or hexagonal-like perturbative coupling.

separated by a thin dielectric layer up to and above room temperature under suitable conditions.[1,2] In this article we have begun to explore the design space under which such condensates can be formed and exploited. We have used a mean-field theory treatment of interlayer exchange interactions within an atomistic tight-binding model of two graphene monolayers layers separated by a dielectric tunnel barrier. This model goes beyond that of earlier continuum treatments, yet provides general agreement for properties that can be evaluated with both models.

We first explored the strength of "spontaneously formed" interlayer condensates and resulting energy gaps in the absence of bare single particle coupling as a function of engineerable parameters including spacing and dielectric constant, of perhaps gate-controllable degree of electron-hole charge concentrations and balance or imbalance between the layers, and of temperature. It is clear, e.g., that the use of low-κ dielectrics is optimum for this purpose, in contrast to use of high-κ dielectrics as optimal for gate-to-channel coupling in MOSFETs, and that there would be a trade-off between condensate strength and the possibility of gate control thereof.

Interlayer coherence, however, is never truly spontaneous because other processes such as single-particle tunneling between layers always couple to the condensate and select a preferred pattern of interlayer phases. For the considered exchange coupling to produce a steady-state interlayer current, such as for the previously proposed BiSFET, some bare interlayer coupling is actually required to allow the condensate to carry a steady-state collective interlayer current. Here, using a perturbative approach, we focused on the maximum value of the condensate-enhanced interlayer current, the critical current, as a function of the bare coupling. Although the bare coupling is treated simply as a parameter here, the results clearly indicated that the critical current may be sensitive to not only the strength of the interlayer coupling, but its detailed nature in this weak coupling limit. It should be noted, however, that in the presence of more significant if still moderate bare coupling, energetically favorable solutions for the combined Hamiltonian could take on the character more in line with the bare coupling, which would have a profound effect on the corresponding critical currents. If electrical devices based on tunnel currents in excitonic condensate systems are to be made in the future, it will be necessary to achieve an adequate degree of control over interlayer tunneling processes.

ACKNOWLEDGMENTS

This work was supported in part by the NRI SWAN Center and the Welch Foundation.

[1] H. Min, R. Bistritzer, J.-J. Su, and A. H. MacDonald, Phys. Rev. B **78**, 121401 (2008).
[2] C.-H. Zhang and Y. N. Joglekar, Phys. Rev. B **77**, 233405 (2008).
[3] I. B. Spielman, J. P. Eisenstein, L. N. Pfeiffer, and K. W. West, Phys. Rev. Lett. **84**, 5808 (2000).
[4] J. P. Eisenstein and A. H. MacDonald, Nature (London) **432**, 691 (2004).
[5] Graphene's valley degeneracy is unfavorable for exciton condensation when interactions are weak, see for example M. Y. Kharitonov and K. B. Efetov, Phys. Rev. B **78**, 241401(R) (2008); R. Bistritzer, H. Min, J. J. Su, and A. H. MacDonald, arXiv:0808.1310 (unpublished); M. Y. Kharitonov and K. B. Efetov, arXiv:0903.4445 (unpublished); The present paper does not attempt to achieve more definitive estimates of the phase diagram of strongly interaction electron-hole systems in graphene bilayers, and focuses instead on properties of the exciton condensate state.
[6] S. K. Banerjee, L. F. Register, E. Tutuc, D. Reddy, and A. H. MacDonald, IEEE Electron Device Lett. **30**, 158 (2009).
[7] International Technology Roadmap for Semiconductors, 2009 update. Available from http://www.itrs.net/
[8] See for example, G. Roberts and A. Sedra, *SPICE*, 2nd ed. (Oxford University Press, New York, 1996).
[9] S. K. Banerjee, L. F. Register, A. H. MacDonald, D. Reddy, and E. Tutuc, BiSFET patent disclosure.
[10] D. Reddy, L. F. Register, E. Tutuc, A. H. MacDonald, and S. K. Banerjee, *Bilayer pseudoSpin field effect transistor (BiSFET): A proposed logic device and circuits*, Device Research Conference, June 2009, pp. 67-68.; D. Reddy, L. F. Register, E. Tutuc, and S. K. Banerjee, IEEE Trans. Electron Devices **57**, 755 (2010).
[11] E. Tutuc, M. Shayegan, and D. A. Huse, Phys. Rev. Lett. **93**, 036802 (2004); M. Kellogg, J. P. Eisenstein, L. N. Pfeiffer, and K. W. West, *ibid.* **93**, 036801 (2004).
[12] L. Tiemann, W. Dietsche, M. Hauser, and K. von Klitzing, New J. Phys. **10**, 045018 (2008).
[13] J.-J. Su and A. H. MacDonald, Nat. Phys. **4**, 799 (2008).
[14] J.-J. Su and A. H. MacDonald, Phys. Rev. B **81**, 184523 (2010).
[15] G. F. Giuliani and G. Vignale, *Quantum Theory of the Electron Liquid* (Cambridge University Press, Cambridge, England, 2005).
[16] R. Saito, G. Dresselhaus, and M. Dresselhaus, *Physical Properties of Carbon Nanotubes* (Imperial College Press, London, 1998).
[17] E. H. Hwang, B. Yu-Kuang Hu, and S. Das Sarma, Physica E (Amsterdam) **40**, 1653 (2008).
[18] T. Sugino, T. Tai, and Y. Etou, Diamond Relat. Mater. **10**, 1375 (2001).
[19] Several low-κ materials with ε_r lower than 3.9 are used in the semiconductor processing flow, e.g., Applied Materials uses C doping in SiO_2 to achieve ε_r in the range 2.5 to 3 in their CVD based Black Diamond® product (http://www.appliedmaterials.com/).
[20] C. R. Dean, A. F. Young, I. Meric, C. Lee, L. Wang, S. Sorgenfrei, K. Watanabe, T. Taniguchi, P. Kim, K. L. Shepard, and J. Hone, arXiv:1005.4917 (unpublished).